Published in final edited form as:
Macromolecules. 2012 November 27; 45(22): 8982–8990. doi:10.1021/ma302206g.

Analysis of Lanthanide Complex Dendrimer Conjugates for Bimodal NIR and MRI Imaging

Christopher M. Andolina[†], **Piper J. Klemm**[‡], **William C. Floyd III**[‡], **Jean M. J. Fréchet**[‡], and **Kenneth N. Raymond**[†,‡,*]

[†]Chemical Sciences Division, Lawrence Berkeley National Laboratory, Berkeley, California 94720

[‡]Department of Chemistry, University of California, Berkeley, California 94720

Abstract

Advances in clinical diagnostic instrumentation have enabled some imaging modalities to be run concurrently. For diagnostic purposes, multimodal imaging can allow for rapid location and accurate identification of a patient's illness. The paramagnetic and near Infra-red (NIR) properties of Dy(III) and Yb(III) are interesting candidates for the development of bimodal NIR and magnetic resonance imaging (MRI) contrast agents. To enhance their intrinsic bimodal properties, these lanthanides were chelated using the hexadentate-all-oxygen-donor-ligand TREN-*bis*-(1-Me)-3,2-HOPO-TAM-NX (**NX,** where X = 1, 2 or 3) and subsequently conjugated to the esteramide dendrimer (**EA**), to improve bioavailability, solubility, and relaxivity. Of these new complexes synthesized and evaluated, **DyN1-EA** had the largest ionic T_1 relaxivity, 7.60 mM^{-1} s^{-1}, while **YbN3-EA** had the largest ionic T_2 relaxivity with a NIR quantum yield of 0.17 % when evaluated in mouse serum. This is the first Yb(III) bimodal NIR/T_2 MRI contrast agent of its kind evaluated.

Introduction

Successful, rapid, and precise diagnostic imaging of soft tissue has relied heavily on magnetic resonance imaging (MRI) for the last three decades. A large portion of MRI's diagnostic popularity can be attributed to injectable contrast agents (CA), which improve the image contrast between healthy and pathological tissue. This enhancement of the image contrast allows radiologists and other medical professionals to quickly identify anomalies such as cancerous tumors, atherosclerosis, spinal deformities, or other soft tissue injuries and diseases.[1–4] As the magnetic strength of clinical MRI instruments increases to 125 MHz, Gd(III) based T_1 contrast agents become less effective at influencing proton exchange.[5, 6] Therefore, development of MRI-CA alternatives to Gd(III) are currently being explored.[7–10] Unique MRI-CA imaging capabilities can be further enhanced by utilizing intrinsic properties of lanthanides for multimodal imaging. Lanthanide complexes have many unique magnetic and luminescent properties, which have allowed researchers to develop effective commercial MRI-CA or luminescent probes for cellular imaging applications that are independent of each other. In this work, we assess and characterize MRI-CA that are potentially bimodal MRI/optical imaging probes. These new lanthanide(III) based MRI-CA with near Infra-red (NIR) imaging capabilities are being explored for the effectiveness both alone and in tandem with already clinically common imaging modalities.[11–15]

[*]To whom correspondence should be addressed: raymond@socrates.berkeley.edu.

Supplemental Information. Characterization of SmNX and EuNX dendrimer conjugates and representative quantum yield plots for YbNX-EA conjugates in all aqueous solutions. This material is available free of charge via the Internet at http://pubs.acs.org.

All current commercial T_1 MRI-CA are based on the well-studied Gd-DTPA and Gd-DOTA complexes and their derivatives (Scheme 1).[16–18] These nitrogen and oxygen donor heteroatom chelators are inefficient as MRI-CAs, as the Gd-DTPA and Gd-DOTA T_1 relaxivities are a modest 3.3 and 3.0 $mM^{-1}s^{-1}$ (at 37.0 °C and 60 MHz), respectively, which requires the injection of gram quantities of MRI-CA to obtain a suitable contrast in the image.[16] These large quantities of injected CA have presented problems such as nephrogenic systemic fibrosis (NSF) for a small percentage of MRI patients with severe kidney dysfunction.[16, 19, 20]

Currently T_1 MRI contrast agents dominate the clinical market worldwide and T_2 contrast agents have limited representation.[7, 21] Many of these T_2 MRI-CA used for clinical diagnostics are iron oxide particles, which are not widely used.[22] Regardless, T_2 (negative mode imaging) is useful for diagnostics of the brain and spinal tissue; as well as other organs and circulatory pathways. It is expected that additional safe and injectable agents would be more widely used if available.[9] We have previously demonstrated that Yb(III) and Dy(III) hexadentate complexes loaded onto dendrimers are T_2 active and potential non-toxic competitors of the superparamagnetic iron oxide MRI-CAs.[8, 10, 21] Utilizing another accessible mode of imaging available to these lanthanide agents, NIR luminescence, only enhances their diagnostic utility.[8]

Multimodal agents are desired diagnostic reports, especially if more imaging modalities could be utilized without compounding side effects of inducing renal stress. Combining imaging modalities gives clinicians the opportunity to improve their diagnostic assessments by generating more accurate images.[1, 23–27] MRI-CA have been combined with fluorescent dyes (visible or NIR) to create multimodal imaging agents in the laboratory, however, many of these agents lack the stability and bioavailability to be diagnostically useful in the clinic.[11, 14, 28–30]

In addition to developing MRI-CA for T_1 and T_2 imaging,[3, 4, 31, 32] the Raymond laboratory has developed sensitized lanthanide luminescent complexes utilizing many of the luminescent lanthanides.[33–39] These complexes contain bifunctional chelators/chromophores which bind to the lanthanide(III) and act as a light harvesting antennae.[35] Examples include compounds such as 1-hydroxypyridin-2-one (1,2-HOPO), 1-methyl-3-hydroxy-pyridin-2-one (1-Me-3,2-HOPO), 2-hydroxyisophthalamide (IAM) and 2,3-dihydroxyterephthalamide (TAM) bidentate chelating moieties. Since the efficient sensitization of the lanthanides is generally indicated as proceeding through the triplet state of the antenna, which has a specific energy, therefore specific lanthanides must be paired with antennae which are larger in energy (2500–5000 cm^{-1}) than the accepting excited state of the lanthanide.[3, 11, 33, 40] This criteria is important to consider when designing Ln(III) luminescent agents, among other general rules for optimizing quantum yields (Φ_{Tot}) of optical lanthanide probes, ensuring efficient energy transfer to the lanthanide.[40–42]

Even if the optical probes are optimized for large quantum yields, the optical imaging of biological tissue is obstructed by the absorbance of photons caused by biomolecules, such as proteins. The absorbance of the excitation source and the luminescent emission in the visible region of the electromagnetic spectra reduces detection limits and the depth of the photons penetration into and out of tissue.[43] The use of NIR optical probes increases the depth of light penetration, since many of these probes are excited outside of the light absorbing "biological window."[43] Additionally, the emission of NIR based probes such as Yb(III) complexes (λ_{EM} ~ 980 nm) does not have the same degree of competition from the autofluorescence of biological molecules in this region. Time-gated luminescence experiments can further enhance the signal to noise of Yb(III) NIR probes relative to the biological matrix by removing the short-lived autofluorescence, after an excitation

pulse.[37, 44] Careful ligand design must be employed to keep open coordination sites of the lanthanide for coordination of inner-sphere water ligands without diminishing the luminescent emission by non-radiative relaxation of the excited Ln(III) *via* vibronic coupling to X-H oscillators. Only a few papers describe T_1 MRI-CA and luminescent lanthanide complexes for bimodal imaging.[12, 13, 15, 45–47] These articles do not evaluate specific NIR emitting lanthanide complexes for their combined NIR/MRI-CA activity.

Dendrimers developed in the Fréchet laboratory have exhibited high bioavailability through mouse biodistribution studies.[48, 49] In addition, the 40 kDa esteramide dendrimer has high renal excretion over several days as the esteramide core degrades *in vivo* (Figure 1). The large scaffolding and mass of the dendrimer, to which up to eight complexes may be covalently conjugated, decreases the tumbling time of the complex. This in turn enhances the per Ln(III) MRI relaxivity.[2, 50–53] The previously described TREN-*bis*-(1-Me)-3,2-HOPO-TAM MRI-CA was used due to the functionality for conjugation to the dendrimer on the TAM moiety. Scheme 2 depicts the three related ligands TREN-*bis*-(1-Me)-3,2-HOPO-TAM-ethylamine (**N1**), TREN-*bis*-(1-Me)-3,2-HOPO-TAM-ethylamine-ethylamine (**N2**), TREN-*bis*-(1-Me)-3,2-HOPO-TAM-ethylamine-*bis*-ethylamine (**N3**) and the Esteramide dendrimer **(EA)** scaffold, to which the monomers were attached.[8, 48, 54] The effect on the photoluminescent properties of the lanthanide complexes such as (Yb(III)) conjugated to the dendrimer and relaxivities for the development of multimodal (MRI/NIR) agents are discussed below.

Experimental Procedures

General

Unless indicated, all chemicals were purchased from commercial sources and used without further purification. All solvents (excluding water) were stored over 4 Å molecular sieves. Water was distilled and further purified by a Millipore cartridge system ($18.2 \times 10^6\ \Omega \cdot cm$). All organic extracts were dried over anhydrous $MgSO_4$ and solvents removed *in vacuo*. Flash chromatography was performed on Merck Silica Gel (40-7 Mesh). Ion exchange chromatography utilized Phenomenex Strata X-C prepacked columns (pore size 85 Å, particle size 33 μm). ^1H and ^{13}C NMR spectra were recorded on a Bruker AVQ 400 at 400 MHz and 100 MHz or a Bruker AVB 400 at 400 MHz and 100 MHz, respectively; the residual solvent peak was used as an internal reference. Elemental analysis and mass spectra (HR = high resolution; ESI-MS = electrospray ionization mass spectrometry) were performed by the QB3 Mass Spectrometry Laboratory, College of Chemistry at the University of California at Berkeley. All synthetic reactions were performed in an atmosphere of nitrogen, unless otherwise noted.

General synthesis of Dy(III), Eu(III), Gd(III) Sm(III) and Yb(III) complexes

The synthesis and characterization of Gd(III), Dy(III), and Yb(III) complexes has been previously reported and described.(8, 54) In a 10 mL round bottom flask, the appropriate ligand, NX (X = 1, 2 or 3), derivative (*ca.* 0.15 mmol, ~10 mg, 1 *eq.*) was suspended in 10 mL of methanol. A Europium(III) or Samarium(IIII) chloride hexahydrate (99.99%) stock solution (~50.0 mM in methanol, exact concentration confirmed by ICP-OES) was added to 1.05 *eq.* (to ensure complete population of the ligands) and two drops of fresh, dry triethylamine (TEA) were added. The solutions were heated to reflux and stirred overnight. Methanol was removed by *in vacuo*. The resulting white powder was redissolved (applying heat if necessary) in 1.0 mL of dry methanol and diethyl ether was slowly added to precipitate the complex or centrifugation (3 min at 6,000 rpm) was used to remove the complex from solution. The solvent was decanted and the white powder washed diethyl ether and dried under high vacuum overnight. **EuN1:** MS-ESI (M^-) = 819.1610 (819.1610

calc'd.). **EuN2:** MS-ESI (M^-) = 862.2032 (862.2032 calc'd.). **EuN3:** MS-ESI (M^-) = 905.2456 (905.2456 calc'd.). **SmN1:** MS-ESI (M^-) = 818.1595 (818.1595 calc'd.). **SmN2:** MS-ESI (M^-) = 861.2017 (861.2017 calc'd.). **SmN3:** ES-ESI (M^-) = 904.2437 (904.2439 calc'd.).

Dendrimer-Chelate Conjugation

Conjugation of GdN1-EA, GdN2-EA, GdN3-EA were previously reported.(54) Conjugation of **DyN1-EA, DyN2-EA, DyN3-EA, YbN1-EA, YbN2-EA,** and **YbN3-EA** were previously reported.[8]

SmNX-EA and EuNX-EA conjugates

In a typical experiment, to a nitric acid (10 % volume) washed EDTA rinsed glass scintillation vial (25 mL) containing 2.0 mg (0.002 mmol, 1.8 *eq.*) of metal complex was added 5.5 mg (0.0011 mmol by carboxylic acid) of **EA** dendrimer. To this was added 0.75 mg (0.065 mmol, 5.9 *eq.*) each of 4-dimethylaminopyridine (DMAP) and hydroxybenzotriazole (HOBt). The solids were dissolved in 0.5 mL DMSO (dimethyl sulfoxide) and 1.5 mg (0.0078 mmol, 7.1 *eq.*) of EDC (EDAC or EDCI, 1-ethyl-3-(3-dimethylaminopropyl) carbodiimide) were added and the reaction was allowed to stir overnight at room temperature under nitrogen atmosphere. After overnight stirring, the solvent was removed *in vacuo* and solids were taken into 5 mL DCM (dichloromethane). After filtering solids through a 0.45 μm PTFE (polytetrafluoroethylene) filter, the solution was precipitated by addition to 100 mL diethyl ether (anhydrous) to give a light yellow solid. The solids were isolated by centrifugation and residual impurities were removed using a PD-10 size exclusion column to give 5.5 mg (83 %) of the desired conjugate.

Size Exclusion Chromatography (SEC)

The SEC system consisted of two SDV Linear S (5 μm) columns (Polymer Standards Service, 300 × 8 mm) using DMF (dimethyl formamide) with 0.2% LiBr as the mobile phase (1 mL/min) in series with a Waters 515 pump, 717 autosampler, 996 Photodiode Array Detector (210–600 nm), and 2414 differential refractive index (RI) detector. Sample volumes were 100 μL and UV spectra were viewed at 350 nm. Molecular weight calibrations for RI spectra were made using linear polyethylene glycol (PEG) standards with toluene as a reference peak. Sm(III) and Eu(III) loading was quantified by comparing polymer peak integrals in UV spectra with a calibration curve obtained from spectra of known quantities of ligand dissolved in DMF and run under identical conditions.

Dynamic light scattering (DLS)

DLS determined hydrodynamic size and was performed at 25 °C by dissolving samples in 1X PBS buffer to a concentration of approximately 1 mg/mL. After brief vortexing, the samples were filtered over 0.45 μm PTFE filters to remove dust and added to a 0.45 μL quartz cuvette and analyzed using a Zetasizer Nanoseries ZS (Malvern Instruments, UK). Results were repeated in triplicate with averages reported.

Inductively Coupled Plasma-Optical Emission Spectroscopy (ICP-OES)

ICP-OES was performed on a Perkin Elmer Optima 7000 DV on Gd(III), Dy(III), Eu(III) and Yb(III). Standards of Gd(III), Dy(III), Eu(III), and Yb(III) were evaluated from 0.01 to 10 ppm. Samples for analysis were digested in 2% (v/v) trace metal grade nitric acid in Millipore water to measure micromolar concentrations of Gd(III), Dy(III), Eu(III), and Yb(III). All volumetric glassware was acid washed and EDTA rinsed.

Cell Culture Cytoxicity by MTT Assay for Conjugates

HeLa cells were purchased from American Type Culture Collection (ATTC) and plated by the Molecular and Cell Biology Cell Culture Facility at University of California, Berkeley, to 10,000 cells per well. Control samples used were live cells, dead cells, the esteramide dendrimer, and Gd-DTPA, a commercial MRI contrast agent. Solutions of MRI-CA were prepared at a concentration of 1.0 mg/mL in Dulbecco's modification of Eagle's Media (DMEM, with glucose and 10% fetal bovine serum (FBS). Dilutions were made on one plate at the rate of two-fold per well, for eight total dilutions and a final concentration of 0.05 mg/mL of sample. These solutions were transferred in 100 μL dilutions onto HeLa cells, which were already in 100 μL of media. These samples were incubated for 72 h at 37.0 °C and 5% CO_2. After 72 h, 40 μL of thiazolyl blue tetrazolium bromide (98% TLC) was added for a MTT assay at 2.9 mg/mL. These samples were incubated for 30 min at 37.0 °C and 5% CO_2. After 30 min, the cells were aspirated and 200 μL of DMSO added, followed by 25 μL of pH 10.5 glycine buffer (100 mmol glycine and 100 mmol salt). Absorbance was measured at 570 nm on a Molecular Devices plate reader and cytotoxicity determined based on blank live cells and starved cells (terminated by denying media). All results repeated in triplicate and averages reported.

Sample preparation

Lyophilized (Labconco Freeze Dry System, Model 775000, FreeZone 4.5 bench top and console freeze-dry systems) **LnNX-EA** conjugates were dissolved in Millipore water, the buffered solution (HEPES, 4-(2-hydroxyethyl)-1-piperazineethanesulfonic acid, pH = 7.4 and I = 0.1 M NaCl) or mouse serum (Rockland, Normal Mouse Serum, Lot #22406) at a concentration of 1.0 mg/1 mL. Solution for photoluminescent lifetime measurements in deuterated buffer, were prepared by lyophilizing solutions containing the complex to dryness and redissolving in 99.9 % deuterium oxide (Cambridge Isotope Laboratories, Inc) with a final concentration of 1 mg/mL. This procedure was repeated to ensure the majority of water was replaced with heavy water. The pD of the buffered solutions were determined, to ensure the lyophilized samples were at similar pH and pD values.

Relaxivity Studies

T_1 measurements were performed on a Bruker mq60 minispec relaxometer. T_1 was determined at 60 MHz (1.41 T) using an inversion recovery pulse sequence. Temperature controlled at 37.0 °C using a Julabo F25 circulating water bath. Each sample was analyzed by ICP-OES for exact Gd(III), Yb(III), and Dy(III) concentration. The inverse of the longitudinal relaxation time of each sample ($1/T_1$, s^{-1}) was plotted against Gd(III), Yb(III), and Dy(III) concentration (μM) and fit by linear regression ($R^2 > 0.99$). Relaxivity analyses were performed in triplicate (three samples) and reported as an average with the standard deviation as the error. Samples were vortexed prior to analysis to break up potential aggregation of complexes. Instrument Parameters: Scans: 4; Recycle Delay: 18.5 s; Gain: 53; Dummy Shots: 0; Detection mode: real; Bandwidth: Broad, 20,000 kHz; Monoexponential Curve Fitting, Phase Cycling. First Pulse Separation: 5 ms; Final Pulse separation: 18,500 ms, Number of data points for fitting: 20; Delay sample window: 0.05 ms; Sampling Window: 0.02 ms; Time for Saturation Curve Display: 6 s. The error reported in the r_2/r_1 ration was calculated by propagating the errors of the measured r_1 and r_2 values. Relaxivity per Ln(III) was determined using the following Equation 1:

$$\frac{1}{T_{n=1,2}} = \frac{1}{T_{n=1,2}^{Solvent}} + r_{n=1,2}[agent] \quad (1)$$

Photophysical Procedures

Solutions were prepared from the stocks of LnNX-EA described above at concentrations less than or equal to 0.1 abs at 350 nm determined by UV-Vis. This was to ensure all solutions were optically dilute. Measurements were collected 1.0 cm cells in quartz Spectrosil® or equivalent (Starna Cells, Inc.). UV-Visible absorption spectra were recorded on a HP 8543 diode array absorption spectrometer equipped with a temperature controller at 25.0 °C. Emission spectra were acquired on a HORIBA Jobin Yvon IBH FluoroLog-3 spectrofluorometer equipped with a temperature controller at 25.0 °C described in great detail elsewhere.[37, 56] Quantum yields in the NIR region were determined by the optically dilute method using the following Equation 2;

$$\frac{\Phi_x}{\Phi_r} = \left[\frac{A_r(\lambda_r)}{A_x(\lambda_x)}\right]\left[\frac{I(\lambda_r)}{I(\lambda_x)}\right]\left[\frac{n_x^2}{n_r^2}\right]\left[\frac{D_x}{D_r}\right] \quad (2)$$

where A is the absorbance at the excitation wavelength (λ), I is the intensity of the excitation light at the same wavelength, n is the refractive index and D is the integrated luminescence intensity (900–1125 nm). The subscripts 'x' and 'r' refer to the sample and reference, respectively. The reference used in this study was $Yb(TTA)_3(H_2O)_2$ in degassed toluene (HPLC grade) as a standard (Φ_r = 0.35 %)(37, 57–59) An estimated error, for measured quantum yields, using this standard is ±25 %. Refractive index values of n =1.33 (sample in buffered solution) and n =1.49 (toluene) were used. Quantum yields were measured relative to **YbN3-EA** in 0.02 M pH 7.4 HEPES I = 0.10 M NaCl for **YbN3-EA** in mouse serum and Millipore water.

For time-resolved luminescent lifetime measurements, a Sirah Cobra Stretch dye laser (CSTR-LG24, Plasmatechnik Gmbh) pumped by a QuantaRay INDI-HG Nd:YAG (SpectraPhysics, Inc.) was used as the excitation sources for the Yb(III) complexes or Eu(III) conjugates. The Xenon flash lamp was coupled to a double grating excitation monochromator for spectral selection. The dye laser pulse 8–10 ns, with an approximate energy of 10 mJ/pulse (λ_{EX} = 376 nm, Exalite 376 Dye), was routed directly into the sample chamber of the Fluorolog. A portion of this excitation was sampled with a 10% beam splitter, which was focused onto the entrance of a UV-sensitive photodiode (DET210, Thor Laboratories). The small amplitude analogue output from the photodiode was processed into a TAC Start signal (NIM) using a TB-01 pulse converter module from IBH. The output signal from the NIR PMT (Hamamatsu, Inc. H9170-75) was processed using a TB-02 0.5 GHz preamplifier module from IBH, and a 100 MHz Constant Fraction Discriminator (CFD) (Model 6915, Phillips Scientific), yielding appropriate TAC Stop signals (NIM). Signals from the visible spectrum PMT (HORIBA Jobin Yvon IBH, TBX-04-D) These were acquired using a 2 ns PCI Multi Channel Scaling (MCS) card (Model P7888-1E, FAST ComTec GmbH) Signals were acquired using an IBH DataStation Hub photon counting module and data analysis was performed using the commercially available DAS 6 decay analysis software package from HORIBA Jobin Yvon IBH. Goodness of fit was assessed by minimizing the reduced chi squared function, χ^2, and a visual inspection of the weighted residuals. Each trace contained at least 1,000 points and the reported lifetime values result from at least three independent measurements. An estimated error for measured lifetimes is ± 10 %.

Triplet State

GdN1-EA and **GdN2-EA** powders were dissolved in a solution of 4:1 ethanol:methanol at ~1 mg / mL. Solvents were HPLC grade. Solutions containing Gd(III) conjugates were diluted to a concentration with an absorbance 0.1 at 340 nm. Approximately 500 μL of the

diluted was transferred to an NMR tube. The NMR tube was cooled using liquid nitrogen to from a solid glass. The phosphorescence emission spectra were collected using the Fluorolog-322 system and exciting both samples at 340 nm with a bandpass of 4 nm. The emission data was collected in 1 nm increments with a 1 nm bandpass. The zero phonon energy was determined by fitting the phosphorescence peaks to Gaussian functions and selecting the center of the lowest energy phosphorescence peak as the $T_{0\rightarrow0}$. The peaks below 500 nm were previously determined to be fluorescent emission, the spectra present here were not time-gated, therefore the fluorescent peaks are present in the phosphorescence spectra.[36, 37, 44]

Results/Discussion

Synthesis and Characterization

Lanthanide complexes (Scheme 2) were synthesized using previously reported and characterized ligands TREN-bis-(1-Me)-3,2-HOPO-TAM-ethylamine **(N1)**, TREN-bis-(1-Me)-3,2-HOPO-TAM-ethylamine-ethylamine **(N2)**, and TREN-bis(1-Me)-3,2-HOPO-TAM-ethylamine-bisethylamine **(N3)** with either and Europium(III) and Samarium(III) trichloride salt of the relevant metal.[60] Other lanthanide complexes (**DyNX GdNX** and **YbNX**) were prepared as described elsewhere.[49, 55, 61] Lanthanide(III) complexes were conjugated through their amine side chains to the acid functionalities of the dendrimer (**EA**) using carbodiimide coupling chemistry discussed in detail (Scheme 2).[8, 54]

The new conjugates were characterized by size exclusion chromatography (SEC), dynamic light scattering (DLS), relaxivity measurements and inductively coupled plasma optical emission spectroscopy (ICP-OES) following procedures detailed here and in prior work.[49, 55, 58] SEC showed that while the dendrimer itself has no UV activity, after conjugation to **LnNX** complexes UV peaks corresponding to a 40 kDa polymer are observed without any small molecule impurities to impact relaxivity. Results of this standard dendrimer characterization are provided in the supplemental information (Figures S1–19).

Relaxivity

The relaxivity measurements of **LnNX-EA** conjugates are reported in Table 1. The calculated r_1 ($1/T_1$ per millimolar (mM) lanthanide complex) values, for **DyN1-EA** and **DyN2-EA** are approximately twice as the relaxivities of commercial Gd-DOTA and Gd-DTPA (3.0 and 3.3 $mM^{-1}s^{-1}$, respectively) monomers.[16] The **DyN3-EA** conjugate exhibited very poor r_1, 0.56 mM^{-1} s^{-1} compared to the other **DyNX-EA**, Gd-DOTA, Gd-DTPA and the **YbNX-EA** MRI-CA. This observation is consistent with additional steric crowding at the dendrimer center, leading to a change in how the dendrimer “folds up” on itself. The metal center, hindered by sterics, likely slowed water exchange, so that the benefits of dendrimer conjugation could not be utilized by the complex. The **YbNX-EA** conjugates had similar r_1 values, 2.15 to 2.99 mM^{-1} s^{-1} which were slightly lower than current commercial agents (Gd-DTPA and Gd-DOTA) at the same conditions. The r_1 value of **YbN3-EA** was measured in mouse serum and 0.1 M pH 7.4 HEPES buffer to assess alternative environments affects on the relaxivity. From the data in Table 1, the relaxivity of the YBN3-EA conjugate does not significantly change by altering the aqueous media used here.

The observed decrease of the r_1 from **DyN1-EA** to **DyN3-EA** was also observed for the **GdN1-EA**, **GdN2-EA** and **GdN3-EA** analogues.[54] In addition, the r_2 ($1/T_2$ per milimolar (mM) lanthanide) values increase from **DyN1-EA** to **DyN3-EA** this trend is observed for the **GdNX-EA** analogues. However, the **YbNX-EA** complexes do not follow these observations, as all three r_1 values are similar. The r_1 values show little impact on the length and rigidity of the linker while the r_2 value increases from **YbN1-EA**, **YbN2-EA**, to **YbN3-**

EA (Table 1).[8] The observed difference in the r_1 and r_2 trends between the **Dy**/**GdNX-EA** and **YbNX-EA** could be the result of Curie relaxivity, which is described as negligible for Gd(III) and Dy(III), however, has a greater impact on later lanthanides, such Yb(III).[62] Additionally, the difference of the coordination number due to the smaller ionic radius of Yb(III) compared to Dy(III) and Gd(III), or coordination geometry may influence these observations.

As discussed in detail elsewhere,[8] examination of the ratio of r_2/r_1 gives an indication of the effectiveness of the conjugate as a T_2 agent with current clinical MRI pulse sequences. Although the **GdNX-EA** r_2 and r_1 values are larger than any of the other **LnNX-EA**, resulting from the more prominent paramagnetic character caused by the seven unpaired *f*-electrons of Gd(III) the ratio of r_2/r_1 not the largest observed. **YbN3-EA** and **YbN2-EA** had the largest ratios 7.69 ± 0.08 and 5.7 ± 0.6, respectively, comparable to the iron oxide clinical nanoparticle, Ferridex®, with a ratio of 6.6. All three **LnN3-EA** conjugates had the largest observed ratios. The **YbN3-EA** and **YbN2-EA** are likely to be the best performing T_2 contrast agents. The r_2/r_1 ratio does not vary when the **YbN3-EA** is measured in either HEPES buffer (pH = 7.4) or mouse serum 7.74 ± 0.26 and 7.82 ± 0.23, respectively. This large r_2/r_1 ratio may indicate similar performance of the **YbN3-EA** *in vivo*, and potential use as a clinical T_2 agent.

Cell Studies

The cell toxicity of the conjugates was determined using *in vitro* cytotoxicity studies by the MTT assay and compiled in Table 2. Cytotoxicity was not observed to HeLa cells, up to 3.0 mg/mL of any conjugate (the highest concentration evaluated), over 72 h at 37 °C and 5% CO_2. The EA dendrimer has previously exhibited low toxicity in mice,[49] and in addition, high solubility in buffered solution. Biodistribution previously conducted on Gd-TREN-bis-(1-Me)-3,2-HOPO-TAM moieties (not conjugated to a dendrimer) with similar functionalities[63] produces suitable biodistribution as an injectable MRI contrast agent. The cytotoxicity determined in this work is consistent with the low toxicity of similar lanthanide dendrimer conjugates previously reported.[8] Lanthanide conjugates containing Dy, Eu, Gd, Sm or Yb(III) have low cytotoxicity in HeLa cells.[8]

Photoluminescence Studies

Photoluminescence characterization of the all lanthanide conjugates is discussed here. The sensitized photoluminescent properties such as quantum yield, Φ_{Tot}, of the conjugates containing lanthanides other than **YbNX-EA**'s were unable to be determined. This is not surprising since the 1-Me-3,2-HOPO is not an efficient sensitizer of Dy(III), Eu(III) or Sm(III). However, data collected by directly exciting europium(III) in the **EuNX-EA** conjugate were utilized to elucidate the speciation lanthanides loaded on to the dendrimer through the recovered time-resolved photoluminescent lifetimes. No photoluminescent data were collected for Sm(III) complexes, as a result of inefficient energy transfer from the chromophores to the Sm(III) center.

The phosphorescent triplet state zero phonon energy, $T_{0\rightarrow0}$, of the two dendrimer complexes were measured using the **GdN1-EA** and **GdN2-EA** conjugates at low temperature (77 K) in an ethanol:methanol solution (4:1 by volume).[34, 49] The phosphorescent spectra of **GdN1-EA** and **GdN2-EA** reveal the $T_{0\rightarrow0}$ energy level of the triplet to be 545 nm (18350 cm^{-1}) and 551 nm (18150 cm^{-1}), respectively (Figure S19). The $T_{0\rightarrow0}$ energy level has been determined to be an important factor in the energy transfer efficiency for sensitized lanthanide complexes.[35, 64] The lowest lying triplet energy level ($T_{0\rightarrow0}$) of the TAM and 1-Me-3,2-HOPO are too low in energy (~19,000 cm^{-1} and ~19,300 cm^{-1}, respectively) to efficiently transfer energy to the visibly emitting lanthanides (such as Dy(III), Tb(III),

Eu(III) and Sm(III)), which have lowest lying excited states above ~20,000 cm^{-1}.[36, 65–67] The TAM chelator/chromophore may also interfere with the emission of the Ln(III) *via* deactivation of the excited Ln(III) and subsequent back energy transfer to the chromophores.[6, 64] However, the $T_{0\rightarrow0}$ energy (for both chromophores) is of the correct quantity to sensitize Yb(III), a NIR emitting Ln(III), the $^2F_{5/2}$ accepting state energy is approximately 10,000 cm^{-1}. Although the chromophores' $T_{0\rightarrow0}$ values are different from the previously reported values by ~ 10 %, this observation is likely caused by differences of the ligand composition. The **GdN1-EA** conjugates show a strong fluorescence peak (*ca.* 420 nm)[36], while the **GdN2-EA** shows a smaller fluorescence peak at the same wavelength. The general similarities in the phosphorescence spectra of **GdN2-EA** and **GN1-EA** are the same for **GdN3-EA** since the electronic configuration of chromophores are not conjugated to the dendrimer, thereby, insulating the chromophores' (1-Me-3,2-HOPO and TAM) electronic states.

Photophysical measurements were collected for the **YbNX-EA** dendrimers and are compiled in Table 3. The quantum yields, Φ_{Tot} (%), were determined to be 0.011, 0.12 and 0.13 % for **YbN1-EA**, **YbN2-EA** and **YbN3-EA** using $Yb(TTA)_3(H_2O)_2$ in degassed toluene as a standard (Φ_r = 0.35 %).[57, 58] The quantum yield for the **YbN3-EA** complex indicates the largest photon efficiency, the ratio of photons into and out of the complex, for all of the Yb complexes. However, the variation for the measured quantum yields of the three conjugates do not scale linearly with the concentration of Yb(III) determined from ICP-OES analysis (reflected in the loading value, Table 3). When the quantum yields are normalized to the loading numbers the difference of the average quantum yields for each conjugate are elucidated (Table 3) showing the **YbN3-EA** and **YbN2-EA** conjugates are the most luminescent while the **YbN1-EA** dendrimer is the least luminescent (Figure S20 and Figure S21). The significant difference of these quantum yields could be a result of different local environments that the Yb centers are located. Many factors are known to influence the quantum yield efficiency of Ln(III) complexes such as the triplet state energy level relative to the accepting excited state of the Ln(III), coordination geometry and proximity of X-H oscillators, to list a few.[35, 64, 68–72] Since the chromophores are nearly identically for each of the complexes and have similar $T_{0\rightarrow0}$ values, the coordination geometry, different organization of the dendrimer conjugate or X-H oscillator quenching must play a pivotal role in the measured quantum yield discrepancy.[60]

The photoluminescence time-resolved lifetimes determined were utilizing an external Sirah dye laser routed into the Fluorolog-322 system. The number of directly coordinated water molecules, q_{H2O} number, were calculated for each conjugate using the empirical equation developed by Beeby and coworkers.[73] The calculated q_{H2O} values for all of the **YbNX-EA** conjugates were less than one-half of a water molecule (Table 3). These non-zero q_{H2O} values suggest an equilibrium between a q = 0 and q = 1 complexes. These small q_{H2O} numbers may indicate the coordination of other molecules (non-NX chelators), possibly from the dendrimer to the ytterbium, which exclude innersphere water molecules and yield a calculated q_{H2O} close to zero. Calculated quantum yields are also consistent with q = 0. In addition the quantum yields are large for Yb complexes in aqueous solution.[74, 75]

The T_1 MRI-CA agents generally require bound waters to exchange with the bulk water to observe efficient T_1 relaxation. Typically, the more directly coordinated water molecules to the lanthanide the greater the measured relaxivity (Equation 1). These q_{H2O} numbers for the **YbNX-EA** are not consistent with the measured T_1 relaxivity values for the **GdNX-EA** complexes. Of course, assumptions that the **YbNX-EA** and **GdNX-EA** conjugates have similar coordination number and geometry are being made, even though the smaller lanthanide, Yb(III), would likely have coordination number of 8 whereas the Gd(III) complexes would have 8–9. However, it is possible to observe T_1 relaxivity when a complex

has a $q_{H2O} = 0$ due to the interaction of water molecules hydrogen bonded to coordinating ligands (amides) relaxed by dipolar mechanisms or by closely diffusing water molecules to the Yb(III) center. [76–80] Therefore, effective Yb(III) based bimodal probes can be developed with $q_{H2O} = 0$, which is beneficial for developing kinetically and thermodymanically stable probes.

Time-resolved luminescent lifetimes were collected for the **EuN1-EA**, **EuN2-EA** and **EuN3-EA** loaded dendrimers in aqueous buffer solution (and deuterated buffer), again utilizing the dye laser system (λ_{EX} = 376 nm) to determine the q_{H2O} value (Table 4). These q_{H2O} values for **EuN1**, **EuN2** and **EuN3-EA** conjugates were calculated using the q_{H2O} equation developed by Supkowski and Horrocks to be 2.9, 1.7 and 2.7, respectively.[81] Contributions from oscillators (N-H or O=CNH) other than the directly bound or outer-sphere water molecules were not taken into account. The calculated Eu(III) based q_{H2O} values are more reasonable since these numbers (**EuNX-EA**) validate the T_1 relaxivities of the **GdNX-EA** analogues unlike the **YbNX-EA** complexes. A single water molecule difference could be explained by the difference of ionic radii for Eu(III) and Yb(III), leading to a lower overall coordination number of 8 for Yb(III), however, this is not observed. A clear physical explanation for the difference between the **YbNX-EA** and **EuNX-EA** conjugates' q_{H2O} will unknown until solution structures are solved.

Examination of the luminescence emission spectra reveals similar bands structures for **YbN1-EA**, **YbN2-EA** and **YbN3-EA** (Figure 2, right panel). The **YbN1-EA** is weakly luminescent even though all conjugates were excited at the same absorbance (340 nm 0.06 abs, Figure, left panel) on the same day. This difference of luminescence efficiency, discussed above, further demonstrates the lower emission of the **YbN1-EA** conjugate. The **YbN3–EA** conjugate has a more pronounced absorbance at 280 nm than the other conjugates. However, no Yb(III) emission was detected by exciting at this wavelength (280 nm), likely indicating an impurity in the sample.

The quantum yield of the **YbN3-EA**, the conjugate with the largest Φ_{Tot}, was measured also in Millipore water (unbuffered) and in mouse serum to determine the effect on not only the relaxivity, but on the luminescence as well. Larger quantum yields were determined in pure water (0.16 %) and in mouse serum (0.17 %) relative the HEPES buffer medium (Table 5). Luminescent time-resolved measurements were collected on one sample (Abs_{340} = 0.1) for each solvent system. Figure shows similar band features in all samples and some variation in the UV-Vis spectra above 300 nm. The UV-Vis absorbance at 378 nm is attributed to the TAM moiety the absorbance transition at ~345 nm is the $\pi \rightarrow \pi^*$ transition of the 1-Me-3,2-HOPO.(37) The contaminant with an UV-Vis absorbance at ~280 nm is observed in these samples as well.

The luminescence emission profiles for **YbN3-EA** in H_2O, HEPES buffer and mouse serum (Figure, right) show the same profile regardless of the aqueous solution, yet different intensities. The **YbN3-EA** spectra were excited at the same absorbance (340 nm ~0.06 abs, Figure, left panel) on the same day. The corresponding emission spectra to the UV-Vis spectra for are shown in Figure (right panel). The **YbN3-EA** conjugate appears more luminescent in mouse serum and Millipore H_2O than in HEPES buffer. The calculated quantum yields validate this claim as well. Why this difference is observed is unclear. However, it is promising that the quantum yield of **YbN3-EA** was enhanced in mouse serum relative to buffer solution.

Conclusions

All **LnNX-EA** conjugates examined here are non-toxic to HeLa cells. Evaluation of the data collected on the **LnNX-EA** conjugates indicates that **YbN3-EA** is the most active agent for T_2 MRI based upon the r_2/r_1 ratio. NIR/visible sensitized photoluminescence measurements indicate no detectable sensitization for Dy, Sm or **EuNX-EA** conjugates. The conjugates **YbN2-EA** and **YbN3-EA** have the largest NIR quantum yields. The **YbN3-EA** is the most promising as an efficient bimodal agent examined here. Continuing development of T_2 agents utilizing Dy(III) and Yb(III) will lead to improved bimodal NIR and MRI lanthanide imaging agents. To our knowledge we have evaluated the first lanthanide bimodal T_2 and NIR imaging agents.

Supplementary Material

Refer to Web version on PubMed Central for supplementary material.

Acknowledgments

The authors acknowledge NIH Grant R01 EB 002047, NIH Grant HL069832, work at LBNL is supported by the Director, Office of Science, Office of Basic Energy Sciences, DOE under Contract DE-AC02-05CH11231, Professor Christopher J. Chang for use of 60 MHz relaxometer, and Adam D. Hill for assistance.

References

1. Skajaa T, Cormode DP, Falk E, Mulder WJM, Fisher EA, Fayad ZA. Arterioscler Thromb, Vasc Biol. 2010; 30:169–176. [PubMed: 19815819]
2. Bumb A, Brechbiel MW, Choyke P. Acta Radiol. 2010; 51:751–67. [PubMed: 20590365]
3. Raymond KN, Pierre VC. Bioconjugate Chem. 2005; 16:3–8.
4. Thompson MK, Misselwitz B, Tso LS, Doble DM, Schmitt-Willich H, Raymond KN. J Med Chem. 2005; 48:3874–7. [PubMed: 15916439]
5. Blockley NP, Jiang L, Gardener AG, Ludman CN, Francis ST, Gowland PA. Magn Reson Med. 2008; 60:1313–20. [PubMed: 19030165]
6. Werner EJ, Kozhukh J, Botta M, Moore EG, Avedano S, Aime S, Raymond KN. Inorg Chem. 2009; 48:277–86. [PubMed: 19032045]
7. Bulte JW, Kraitchman DL. NMR Biomed. 2004; 17:484–99. [PubMed: 15526347]
8. Klemm PJ, Floyd WC III, Andolina CM, Fréchet JMJ, Raymond KN. Eur J Inorg Chem. 2012:2108–2114.
9. Laurent S, Forge D, Port M, Roch A, Robic C, Vander Elst L, Muller RN. Chem Rev. 2008; 108:2064–110. [PubMed: 18543879]
10. Norek M, Peters JA. Prog Nucl Magn Reson Spectrosc. 2011; 59:64–82. [PubMed: 21600356]
11. Brooksby B, Pogue BW, Jiang S, Dehghani H, Srinivasan S, Kogel C, Tosteson TD, Weaver J, Poplack SP, Paulsen KD. Proc Natl Acad Sci USA. 2006; 103:8828–8833. [PubMed: 16731633]
12. Pellegatti L, Zhang J, Drahos B, Villette S, Suzenet F, Guillaumet G, Petoud S, Toth E. Chem Commun. 2008:6591–3.
13. Tallec G, Imbert D, Fries PH, Mazzanti M. Dalton Trans. 2010; 39:9490–2. [PubMed: 20830407]
14. Frullano L, Meade TJ. J Biol Inorg Chem. 2007; 12:939–49. [PubMed: 17659368]
15. Koullourou T, Natrajan LS, Bhavsar H, Pope SJ, Feng J, Narvainen J, Shaw R, Scales E, Kauppinen R, Kenwright AM, Faulkner S. J Am Chem Soc. 2008; 130:2178–9. [PubMed: 18220401]
16. Port M, Idee JM, Medina C, Robic C, Sabatou M, Corot C. BioMetals. 2008; 21:469–90. [PubMed: 18344005]
17. Caravan P. Chem Soc Rev. 2006; 35:512–23. [PubMed: 16729145]

18. Caravan P, Ellison JJ, McMurry TJ, Lauffer RB. Chem Rev. 1999; 99:2293–352. [PubMed: 11749483]
19. Yantasee W, Fryxell GE, Porter GA, Pattamakomsan K, Sukwarotwat V, Chouyyok W, Koonsiripaiboon V, Xu J, Raymond KN. Nanomedicine. 2010; 6:1–8. [PubMed: 19447204]
20. Zou Z, Ma L. Indian J Dermatol. 2011; 56:65–73. [PubMed: 21572796]
21. Na HB, Song IC, Hyeon T. Adv Mater. 2009; 21:2133–2148.
22. Mentlein R, Schlorf T, Meincke M, Kossel E, Gluer CC, Jansen O. Int J Mol Sci. 2011; 12:12–23. [PubMed: 21339973]
23. Yang J, Lim E-K, Lee HJ, Park J, Lee SC, Lee K, Yoon H-G, Suh J-S, Huh Y-M, Haam S. Biomaterials. 2008; 29:2548–2555. [PubMed: 18329706]
24. Mulder WJM, Strijkers GJ, van Tilborg GAF, Cormode DP, Fayad ZA, Nicolay K. Acc Chem Res. 2009; 42:904–914. [PubMed: 19435319]
25. Kim J, Piao Y, Hyeon T. Chem Soc Rev. 2009; 38:372–390. [PubMed: 19169455]
26. Mulder WJM, Cormode DP, Hak S, Lobatto ME, Silvera S, Fayad ZA. Nat Clin Pract Cardiovasc Med. 2008; 5:S103–S111. [PubMed: 18641599]
27. Hüber MM, Staubli AB, Kustedjo K, Gray MHB, Shih J, Fraser SE, Jacobs RE, Meade TJ. Bioconjugate Chem. 1998; 9:242–249.
28. Koyama Y, Talanov VS, Bernardo M, Hama Y, Regino CAS, Brechbiel MW, Choyke PL, Kobayashi H. J Magn Reson Imaging. 2007; 25:866–871. [PubMed: 17345640]
29. Bumb A, Regino CA, Perkins MR, Bernardo M, Ogawa M, Fugger L, Choyke PL, Dobson PJ, Brechbiel MW. Nanotechnology. 2010; 21:175704. [PubMed: 20368682]
30. Mulder, WJM.; Strijkers, GJ.; Koole, R.; Donega, CDM.; Storm, G.; Griffioen, AW.; Nicolay, K. Bimodal Liposomes and Paramagnetic QD-Micelles for Multimodality Molecular Imaging of Tumor Angiogenesis in Nanoparticles in Biomedical Imaging. Springer; New York: 2007.
31. Datta A, Raymond KN. Acc Chem Res. 2009; 42:938–947. [PubMed: 19505089]
32. Pierre VC, Botta M, Raymond KN. J Am Chem Soc. 2005; 127:504–505. [PubMed: 15643857]
33. D'Aleo A, Moore EG, Szigethy Gz, Xu J, Raymond KN. Inorg Chem. 2009; 48:9316–9324. [PubMed: 19722546]
34. Moore EG, Jocher CJ, Xu J, Werner EJ, Raymond KN. Inorg Chem. 2007; 46:5468–5470. [PubMed: 17567001]
35. Moore EG, Samuel APS. Acc Chem Res. 2009; 42:542–552. [PubMed: 19323456]
36. Moore EG, Szigethy G, Xu J, Pålsson L-O, Beeby A, Raymond KN. Angew Chem Int Ed. 2008; 47:9500–9503.
37. Moore EG, Xu J, Dodani SC, Jocher CJ, D'Aleo A, Seitz M, Raymond KN. Inorg Chem. 2010; 49:4156–4166. [PubMed: 20364838]
38. Moore EG, Xu J, Jocher CJ, Castro-Rodriguez I, Raymond KN. Inorg Chem. 2008; 47:3105–3118. [PubMed: 18311915]
39. Petoud S, Muller G, Moore EG, Xu J, Sokolnicki J, Riehl JP, Le UN, Cohen SM, Raymond KN. J Am Chem Soc. 2007; 129:77–83. [PubMed: 17199285]
40. Sastri, VS.; Bünzli, J-CG.; Rao, R.; Rayudu, GVS.; Perumareddi, JR. Modern Aspects of Rare Earths and Their Complexes. 1. Elsevier B. V; Amsterdam, Netherlands: 2003.
41. Bünzli J-CG. Acc Chem Res. 2006; 39:53–61. [PubMed: 16411740]
42. Bünzli J-CG, Piguet C. Chem Rev. 2002; 102:1897–1928. [PubMed: 12059257]
43. Tromberg BJ, Shah N, Lanning R, Cerussi A, Espinoza J, Pham T, Svaasand L, Butler J. Neoplasia. 2000; 2:26–40. [PubMed: 10933066]
44. Moore EG, Seitz M, Raymond KN. Inorg Chem. 2008; 47:8571–8573. [PubMed: 18729353]
45. Nonat A, Fries PH, Pecaut J, Mazzanti M. Chemistry- A Eur J. 2007; 13:8489–506.
46. Nonat A, Gateau C, Fries PH, Mazzanti M. Chemistry. 2006; 12:7133–50. [PubMed: 16755632]
47. Crich SG, Biancone L, Cantaluppi V, Duo D, Esposito G, Russo S, Camussi G, Aime S. Magn Reson Med. 2004; 51:938–44. [PubMed: 15122675]
48. Lee CC, Gillies ER, Fox ME, Guillaudeu SJ, Frechet JM, Dy EE, Szoka FC. Proc Natl Acad Sci USA. 2006; 103:16649–54. [PubMed: 17075050]

49. van der Poll DG, Kieler-Ferguson HM, Floyd WC, Guillaudeu SJ, Jerger K, Szoka FC, Frechet JMJ. Bioconjugate Chem. 2010; 21:764–773.
50. Nwe K, Milenic D, Bryant LH, Regino CA, Brechbiel MW. J Inorg Biochem. 2011; 105:722–727. [PubMed: 21463567]
51. Sena LM, Fishman SJ, Jenkins KJ, Xu H, Brechbiel MW, Regino CA, Kosaka N, Bernardo M, Choyke PL, Kobayashi H. Nanomedicine. 2010; 5:1183–91. [PubMed: 21039196]
52. Nwe K, Bernardo M, Regino CA, Williams M, Brechbiel MW. Bioorg Med Chem. 2010; 18:5925–31. [PubMed: 20663676]
53. Wiener EC, Konda S, Shadron A, Brechbiel M, Gansow O. Invest Radiol. 1997; 32:748–54. [PubMed: 9406015]
54. Floyd WC III, Klemm PJ, Smiles DE, Kohlgruber AC, Pierre VC, Mynar JL, Frechet JMJ, Raymond KN. J Am Chem Soc. 2011; 133:2390–3. [PubMed: 21294571]
55. Pierre, VC. Chemistry. University of California; Berkeley, Berkeley, CA: 2005.
56. Moore EG, Xu J, Jocher CJ, Corneillie TM, Raymond KN. Inorg Chem. 2010; 49:9928–9939. [PubMed: 20873782]
57. Tsvirko MP, Meshkova SB, Venchikov VY, Bol'shoi DV. Opt Spectrosc (Engl Transl). 1990; 87:866–870.
58. Meshkova SB, Topilova ZM, Bolshoy DV, Beltyukova SV, Tsvirko MP, Venchikov VY. Acta Phys Pol, A. 1999; 95:983–990.
59. Tsvirko M, Meshkova S, Venchikov V, Topilova Z, Bol'shoi D. Opt Spectrosc. 2001; 90:669–673.
60. Pierre VC, Botta M, Aime S, Raymond KN. Inorg Chem. 2006; 45:8355–64. [PubMed: 16999435]
61. Kimura T, Kato Y. J Alloys Compd. 1995; 225:284–287.
62. Helm L. Relaxivity in paramagnetic systems: Theory and mechanisms. Prog Nucl Magn Reson Spectrosc. 2006; 49:45–64.
63. Thompson MK, Misselwitz B, Tso LS, Doble DMJ, Schmitt-Willich H, Raymond KN. J Med Chem. 2005; 48:3874–3877. [PubMed: 15916439]
64. Latva M, Takalo H, Mukkala V-M, Matachescu C, Rodríguez-Ubis JC, Kankare J. J Lumin. 1997; 75:149–169.
65. Carnall WT, Fields PR, Rajnak K. J Chem Phys. 1968; 49:4450–4455.
66. Carnall WT, Fields PR, Rajnak K. J Chem Phys. 1968; 49:4447–4449.
67. Carnall WT, Fields PR, Rajnak K. J Chem Phys. 1968; 49:4424–4442.
68. Beeby A, Dickins RS, Faulkner S, Parker D, Williams JAG. Chem Commun. 1997:1401–1402.
69. Beeby A, Clarkson IM, Dickins RS, Faulkner S, Parker D, Royle L, de Sousa AS, Williams JAG, Woods M. Perkin Trans. 1999; 2:493–504.
70. Haas Y, Stein G, Wurzberg J. J Chem Phys. 1974; 60:258.
71. Horrocks WD, Sudnick DR. Science. 1979; 206:1194–1196. [PubMed: 505007]
72. Choppin GR, Peterman DR. Coord Chem Rev. 1998; 174:283–299.
73. Faulkner S, Beeby A, Dickins RS, Parker D, Williams JAG. J Fluoresc. 1999; 9:45–49.
74. Aebischer A, Gumy F, Bunzli J-CG. Phys Chem Chem Phys. 2009; 11:1346. [PubMed: 19224035]
75. Zhang J, Badger PD, Geib SJ, Petoud S. Angew Chem, Int Ed. 2005; 44:2508.
76. Caravan P, Ellison JJ, McMurry TJ, Lauffer RB. Chem Rev. 1999; 99:2293. [PubMed: 11749483]
77. Aime S, Batsanov AS, Botta M, Howard JAK, Parker D, Senanayake K, Williams G. Inorg Chem. 1994; 33:4696.
78. Botta M. Eur J Inorg Chem. 2000:399.
79. Freed JH. J Chem Phys. 1978; 68:4034.
80. Bottrill M, Kwok L, Long NJ. Chem Soc Rev. 2006; 35:557. [PubMed: 16729149]
81. Supkowski RM, Horrocks WD. Inorg Chim Acta. 2002; 340:44–48.

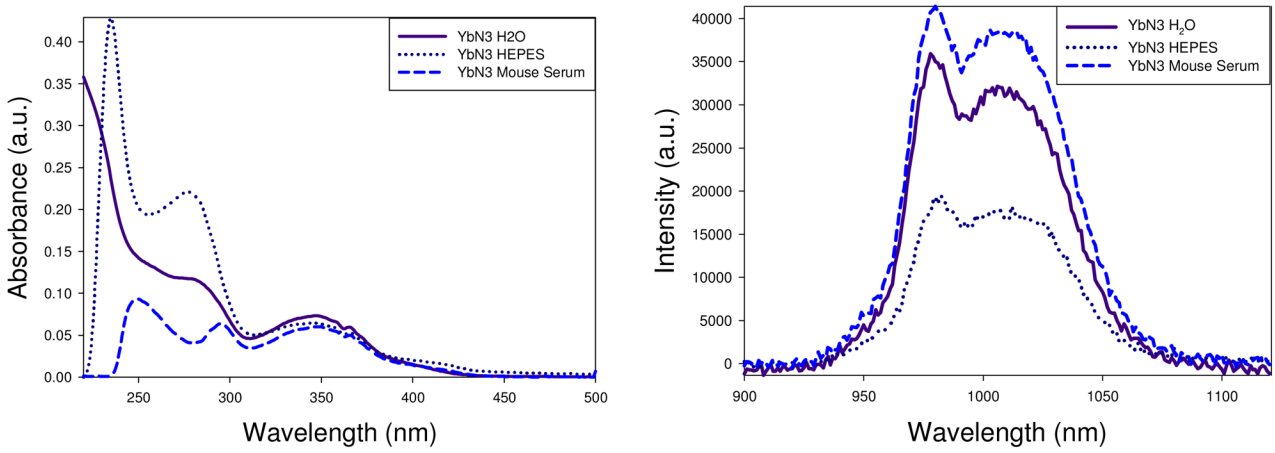

Figure 1.

UV-Vis spectra of **YbN3-EA** in water, HEPES and mouse serum with an absorbance of ~0.06 at 340 nm (left) and corresponding emission spectra λ_{EX} = 340 ± 14.5 nm (emission collected in 1.0 nm increments, 14.5 nm bandpass with an integration time of 1.0 s).

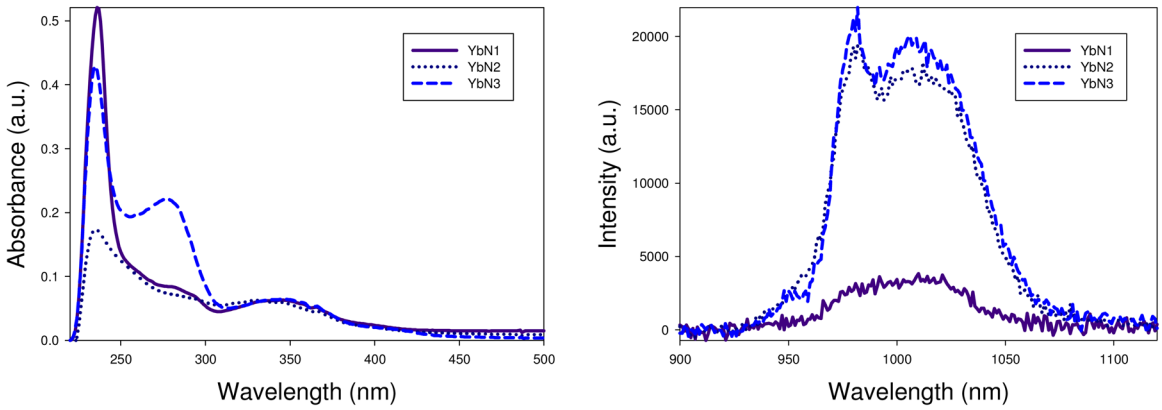

Figure 2.

UV-Vis spectra of **YbN1-EA**, **YbN2-EA** and **YbN3-EA** with an absorbance of 0.06 at 340 nm (left) and corresponding emission spectra λ_{EX} = 340 ± 14.5 nm (emission collected in 1.0 nm increments, 14.5 nm bandpass with an integration time of 1.0 s) collected in aqueous buffer solution.

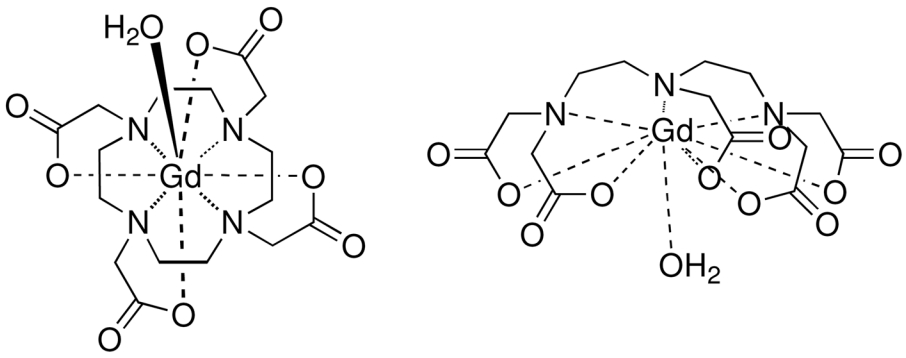

Scheme 1.

The ligand architectures of Gd(III) based commercial MRI contrast agents. Left: Gd-DOTA (Dotarem, Guebert, Inc.). Right: Gd-DTPA (Magnevist, Schering, Inc.). [16, 19, 20]

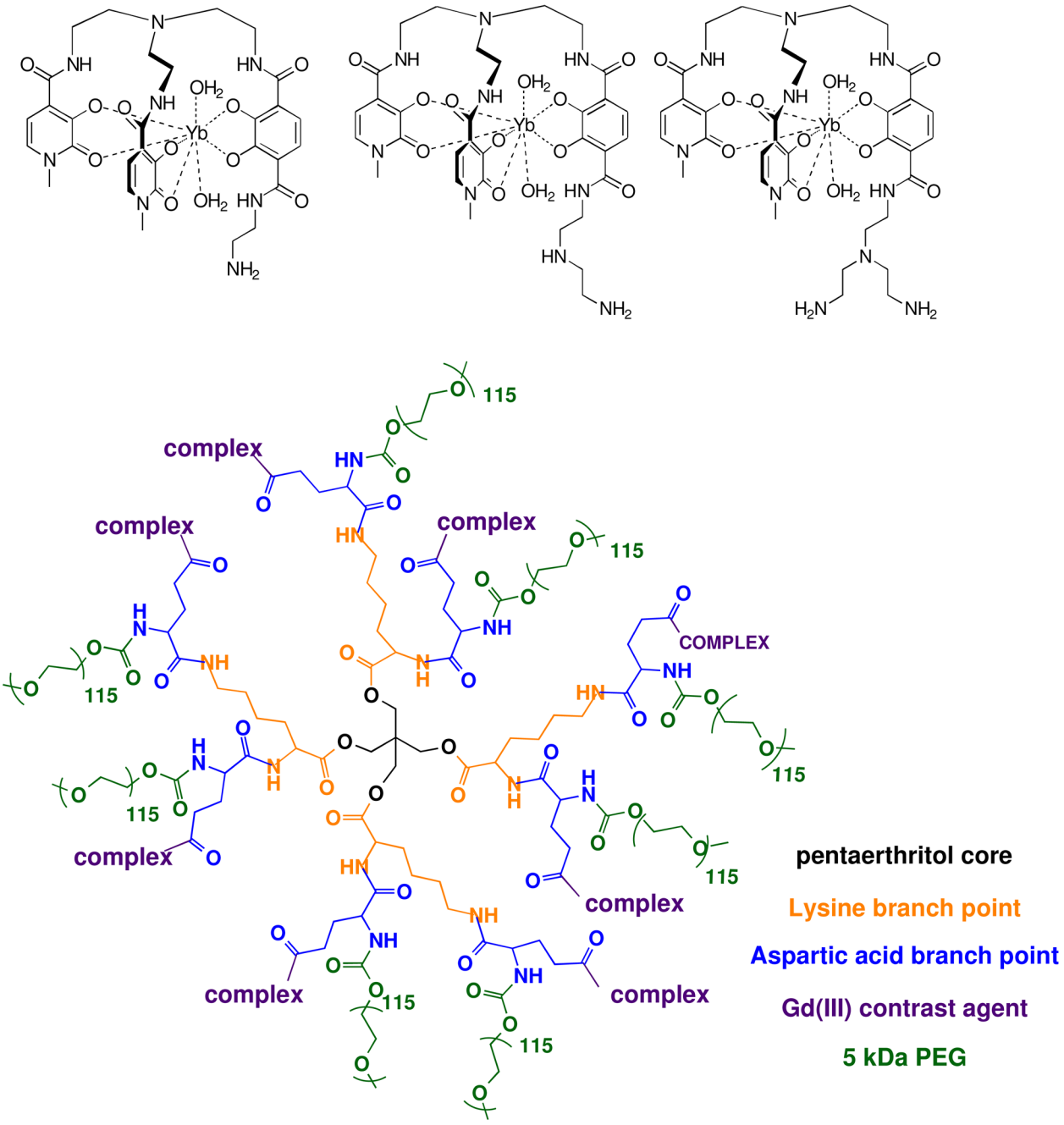

Scheme 2.

Structures of the ligands (**N1**, **N2** and **N3**) used for MRI and NIR imaging agents (top).[54, 55] The Esteramide dendrimer (**EA**) scaffold (bottom).[49]

Table 1

Comparison of the per lanthanide relaxivity, r_1, ($mM^{-1}s^{-1}$) of the lanthanide conjugates in Millipore water (pH = 6), at μM Ln(III) concentrations, (37.0 °C, and 60 MHz).

Complex	r_1 ($mM^{-1}s^{-1}$)	r_2 ($mM^{-1}s^{-1}$)	r_2/r_1
DyN1-EA	7.60(5)	14.1(4)[8]	1.86(5)
DyN2-EA	5.5(3)	5.5(4)[8]	1.0(1)
DyN3-EA	0.56(2)	2.2(1)[8]	3.9(2)
YbN1-EA	2.43(1)	5.6(8)[8]	2.3(3)
YbN2-EA	2.15(2)	12(1)[8]	5.7(6)
YbN3-EA	2.99(2)	23.0(2)[8]	7.69(8)
YbN3-EA (0.1 M HEPES, pH 7.4)	2.96(6)	22.9(6)	7.7(2)
YbN3-EA (mouse serum)	3.04(8)	23.8(3)	7.8(2)
GdN1-EA	38.14(2)[54]	42(1)[8]	1.11(4)
GdN2-EA	31.9(1)[54]	35.1(1)[8]	1.10(1)
GdN3-EA	7.19(7)[54]	23.4(4)[8]	3.25 (6)

Table 2

Cytotoxicity of multimodal mixed lanthanide imaging agents.

Complex: Dendrimer (if applicable) (1.0 mg/mL, unless otherwise noted)	% Viability (After 72 h)
Esteramide Control	99.4(4)
Gd(DTPA) Control	99.6(1)
GdN2-EA, DyN2-EA, and YbN2-EA (3.0 mg/mL)	99.4(2)
EuN1-EA	99.6(2)
EuN2-EA	99.5(1)
EuN3-EA	99.5(3)
SmN1-EA	99.8(9)
SmN2-EA	99.6(1)
SmN3-EA	99.7(2)

Table 3

Photophysical properties of the **YbNX-EA** dendrimers in 0.1 M pH 7.4 HEPES buffer.

Monomer	Loading	λ_{MAX} (nm)	Φ_{Tot} (%)	Φ_{Tot} (%)/ Loading	τ (μs)	τ_{D2O} (μs)	q_{H2O}
YbN1	2^8	344	0.011	0.0015	1.8	16.7	0.30
YbN2	7^8	344	0.12	0.0056	2.6	20.9	0.14
YbN3	6^8	345	0.13	0.0066	2.5	20.3	0.15

Estimated error in Φ_{Tot} and τ are 25% and 10%, respectively. Φ_{Tot} (%) was determined using $Yb(TTA)_3 \cdot 2H_2O$ in toluene as a standard. Lifetimes are the average of three or more samples from the same stock solution. λ_{EX} = 340 ± 14.5 nm and λ_{Em} = 990 ± 14.5 nm each with a 14.5 nm bandpass.

Table 4

Time-resolved luminescent lifetimes of **EuNX-EA** (X = 1, 2 or 3).

Monomer	τ (μs)	τ_{D2O} (μs)	q_{H2O}
EuN1	258	1164	2.9
EuN2	375	1530	1.7
EuN3	297	1311	2.7

Lifetimes are the average of three independent measurement, λ_{EX} = 376 nm, λ_{EM} = 615 ± 10 nm (1 mg/mL) in 20.0 mM HEPES buffer pH = 7.4, *I* = 0.1 M NaCl an estimated error of 10 % is assumed.

Table 5

Photophysical properties of the **YbNX-EA** (X = 1, 2 or 3) HEPES buffer, H_2O and mouse serum.

Monomer	Loading	Solvent	λ_{MAX} (nm)	Φ_{Tot} (%)
YbN3	6	Millipore H_2O	344	0.16
YbN3	6	HEPES pH = 7.4	345	0.13
YbN3	6	Mouse Serum	344	0.17

Estimated error in Φ_{Tot} and τ are 25% and 10%, respectively. Φ_{Tot} (%) was determined using relative to **YbN3-EA** in HEPES buffer. Lifetimes are the average of three or more samples from the same stock solution. λ_{EX} = 340 ± 14.5 nm and λ_{EM} = 990 ± 14.5 nm.